Advances in Science and Technology Research Journal

*Advances in Science and Technology Research Journal* 2022, 16(6), 179–185
https://doi.org/10.12913/22998624/156215
ISSN 2299–8624, License CC-BY 4.0

Received: 2022.10.02
Accepted: 2022.11.17
Published: 2022.12.01

# Performance Analysis of Piezoelectric Energy Harvesting System

Bartłomiej Ambrożkiewicz[1], Zbigniew Czyż[2*], Paweł Stączek[1], Andrés Omar Tiseira[3], Jorge García-Tíscar[3]

[1] Department of Automation, Faculty of Mechanical Engineering, Lublin University of Technology, ul. Nadbystrzycka 36, 20-618 Lublin, Poland

[2] Aeronautics Faculty, Polish Air Force University, ul. Dywizjonu 303 35, 08-521 Dęblin, Poland

[3] CMT-Motores Térmicos, Universitat Politécnica de Valéncia, 46022 Valencia, Spain

* Corresponding author's e-mail: z.czyz@law.mil.pl

**ABSTRACT**

This paper analyzes a piezoelectric system made of a smart lead zirconate material. The system is composed of a monolithic PZT (piezoelectric ceramic) plate made of a ceramic-based piezoelectric material. The experiment was conducted on a test stand with a GUNT HM170 wind tunnel and a special measurement system. The developed bluff-body shape mounted on an elastic beam with a piezoelectric was mounted on a mast with arms. Springs were fixed on the arms to limit the movement of the test object. Air flow velocity in the wind tunnel and forced vibration frequencies were changed during the tests. The recorded parameters were an output voltage signal from the piezoelectric element and linear accelerations at selected points of the test object. The highest energy efficiency of the tested system was specified from mechanical vibrations and air flow. The results of the tests are a resonance curve for the tested system and a correlation of RMS voltage and acceleration as a function of the velocity of air flow for the excitation frequency f ranging from 1 to 6 Hz. The tests specified the area where the highest output voltage under the given excitation conditions is generated.

**Keywords:** hybrid energy harvesting system, macro fiber composite, cross-section design, vortex-induced vibration, galloping

## INTRODUCTION

The global trend in reducing the consumption of fossil fuels leads to finding new sources of green energy. One of them is Energy Harvesting which refers to a process wherein the sources such as mechanical vibrations, temperature gradients, or light are scavenged and converted to obtain small portions of power which can be used as a power supply for remote devices with relatively low-demand power consumption [1]. This paper focuses on the combination of vibrational energy harvesters (VEHs) [2] and systems based on energy scavenging from the airflow [3]. Both of these types can be classified according to the type of energy conversion, namely electromagnetic [4], piezoelectric [5], and electrostatic [6] effects. Since the early 21st century, new designs for energy harvesting systems have been continuously created, and the relevant research results are collected in the reviews [7, 8]. The recent trend is focused on hybrid energy harvesters, or two or more effects or phenomena to scavenge electrical energy, i.e. the piezoelectric and triboelectric effect [9], the piezoelectric and electromagnetic effect [10], piezoelectric effect and water waves [11]. Another hybrid form of energy harvesting system to be discussed here is the system known as aeroelastic that combines the piezoelectric effect and air flow.

Designing new energy harvesting systems takes into account the highest possible power output. The system is then adjusted to operation by its resonance frequency [12] or operating around it by subharmonic solutions [13]. Our previous research [14] attempted to find such a system's design which is prone to the vortex-induced

vibrations (VIVs) effect [15] at relatively low wind velocities and the galloping effect [16] at relatively high wind velocities. The research on wind energy harvesting systems [3, 17] shows that the circular bluff-body has the oscillating solution by vortex-induced vibrations, while the square-shaped body has the highest power output by the galloping effect. To combine both of the mentioned effects and to increase power performance at a wide range of wind velocities, the new design combined both the round and square shapes of the body along its generatrix. The system in such a form was, however, operating at higher wind velocities and was prone to the galloping effect so the modified design is proposed with additional springs to make the system more sensitive to low wind velocities.

The power performance of the system was improved by applying hybrid excitation in form of the air flow in the wind tunnel of variable velocities and mechanical vibrations excited by a shaker. Such double excitation was already discussed by Abdelkefi et al. [18], and its main advantage is the possibility to create a desirable dynamical system of an energy harvester, i.e. an oscillating solution by specific excitation conditions both from wind velocity and a shaker. Such countermeasures make the system more flexible to variable excitation conditions. The main aim of the new design as compared to previous design is to obtain an oscillating solution for low wind velocities. One of countermeasures is the application of additional springs mounted on a beam to change its characteristic frequency and make it more flexible for a wider range of excitations [19]. Referring to the previous research, the test was focused mainly on low wind velocities and the same range of excitation frequencies.

What is worth mentioning is the fact, that Energy Harvesting area is developing quite fast focusing on the optimization problems [20], new designs [21] and new ways of sources of excitations [22]. Definitely, we can state that our system is the new branch in the area of study of piezo-electric energy harvesting systems, which is developing due to the relatively high output voltage/power level by the small deflection of the piezo-patch [23].

## RESEARCH OBJECT & TEST RIG

Figure 1 schematically shows the measurement system with the elements of the test object. The piezoelectric system consists of an aluminum elastic beam, a piezoelectric element, a bluff-body and a spring arm to attach springs whose other ends are connected to the elastic beam. The elastic beam 200 mm long in total is 20×1 mm (width × thickness) in cross-section. The free section of the elastic beam without the attachment point is 160 mm (20 mm for being attached to the sting and 20 mm to the bluff body). The beam was bolted to a support structure that was a vertical aluminum flat bar 20×4 mm (width × thickness) in cross-section. The bluff body spring arm printed from PLA (Polylactide) material and made in 3D printing technology was bolted to the support structure at the height of the bluff body action. The orientation of the bluff body and elastic beam allows for horizontal oscillation. Such a position of the beam results from the induced vortices behind the bluff body.

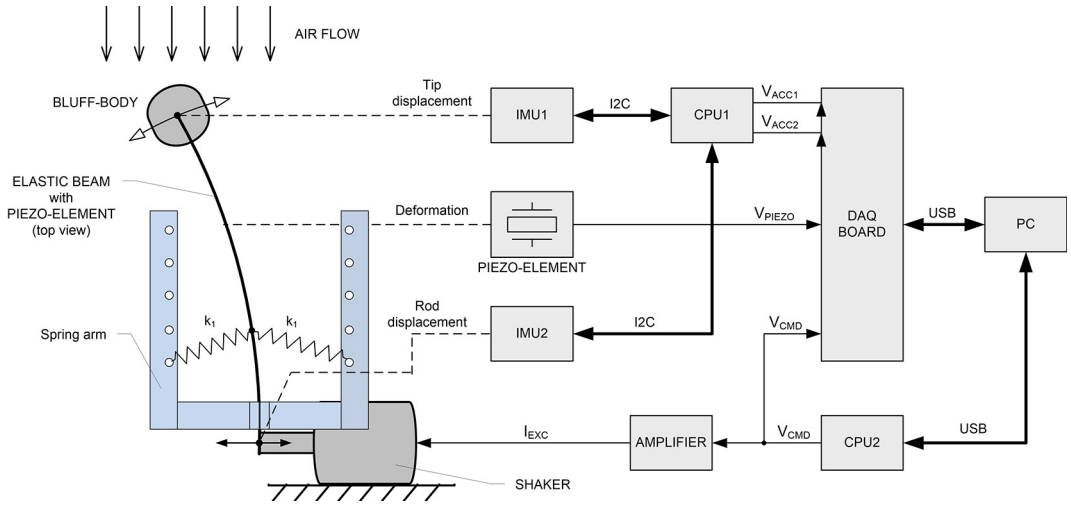


**Fig. 1.** Diagram of the measuring system. The bluff-body within its support and springs are shown in top view

A piezoelectric material used in the research was Macro Fiber Composite™ (MFC) of type P1 by Smart Material Corporation. This sort of piezoelectric material has the following layers: its middle layer is a monolithic PZT plate which is a piezoelectric ceramic and its outer layers are an inter-digitated electrode pattern on polyimide film [24]. The dimensions of this piezoelectric element can be classified as two areas, i.e. an active area of 28×14 mm and an area of 38×20 mm that covers the external dimensions of the entire element. The maximum blocking force is 146 N (±10%). The piezoelectric element can operate in the voltage range from -500 V to +1500 V and its maximum operating frequency is less than 1 MHz. Its typical lifetime is 10E+10 cycles (<600 ppm). It is 300 µm thick and its capacitance is 1.9 nF (±20%). This particular piezoelectric element is described in detail in [14].

Vortices and thus vibrations are induced by the bluff body which is a combination of a cylinder and a cuboid. The geometry was designed in the Solidworks CAD software and then printed with a 3D printer using the Fused Deposition Modeling (FDM) method. The printed tested bluff body was 30.4 g. The shape of its cross-section changed smoothly along its entire length from a square to a circle using the spline function. Importantly, the cross-sectional areas of the square and circle at their ends are identical and equal to 400 mm$^2$. Figure 2 depicts the selected cross-sections of the bluff body and its location in the measurement space of the wind tunnel. The bluff body was 100 mm high.

A GUNT HM 170 open wind tunnel with a closed measurement area was used in the experiment. The wind tunnel is described in detail in [14]. Its measurement section is a square of 300 mm x 300 mm in cross section, and the test object was in the centre. The air flow velocity around the object was controlled in the experiment by varying the speed of a fan installed at the wind tunnel outlet. Figure 3 shows the test object in the measurement space of the wind tunnel. A TIRA S513 vibration generator to excite the elastic beam was under the measurement section. This device has a rated peak force of 100 N and frequency ranging from 2 to 7000 Hz, which enables an axial displacement of 13 mm, a maximum velocity of 1.5 m/s and a maximum acceleration of 45 g. The sinusoidal excitation signal was amplified during the measurements with a TIRA DA 200 digital amplifier.

This research continues the research discussed in [14] that focused on, e.g. the same bluff body but mounted on a freely moving elastic beam. Here, the movement of the elastic beam was modified by the springs attached to its both sides.

## RESULTS AND DISCUSSION

Figure 4 shows the G force as a function of the frequency of vibration forced by the shaker f with no air flow in the wind tunnel. A resonance

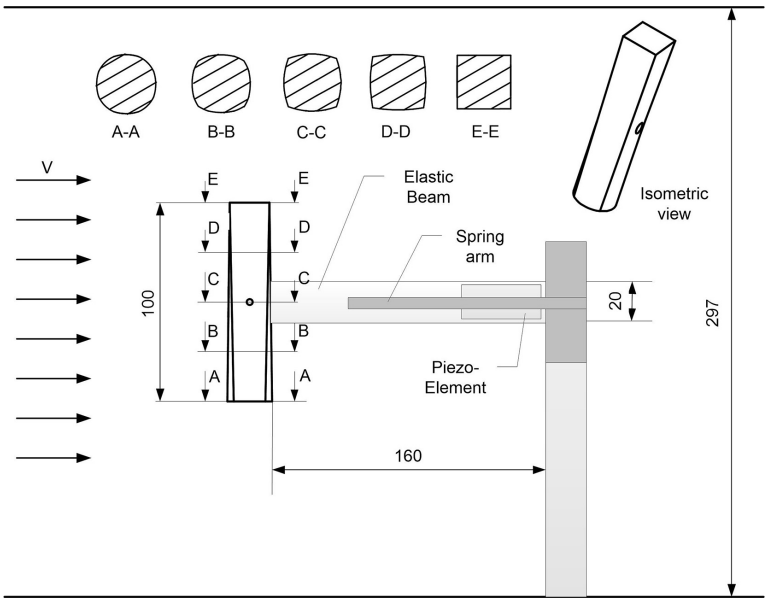


**Fig. 2.** Bluff body geometry and the selected cross-section

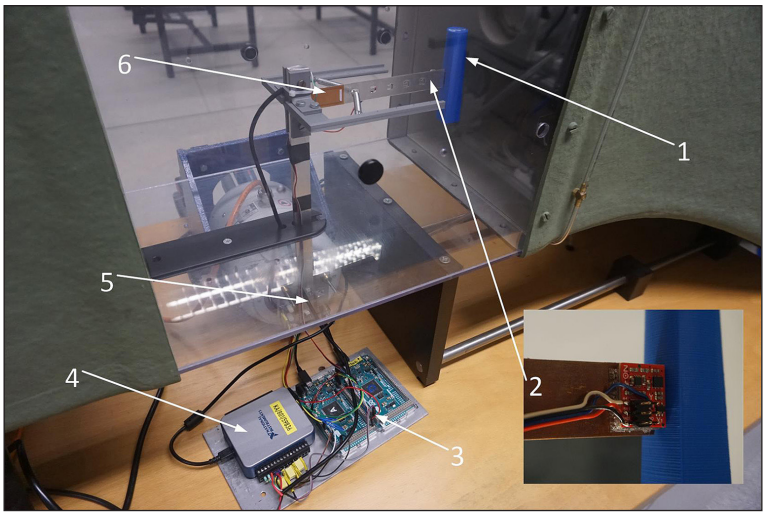


**Fig. 3.** The test object in the measurement section of the wind tunnel, 1 – bluff-body, 2 – three-axis MEMS digital accelerometer module at the tip of the beam (type MMA8452Q, mounted on another side of the beam), 3 – two microcontroller boards, 4 – DAQ card, 5 – accelerometer module (MMA8452Q) mounted on the shaker rod, 6 – piezo-element.

curve for the response of the mechanical system was plotted from this test so that any further research could focus on achieving the highest possible output voltage during hybrid excitation. The tests resulted in specifying the maximum acceleration of the moving bluff-body, i.e. 1.33 g for f = 2.6 Hz, whereas the same value of 0.79 g was recorded for the extreme frequencies of 0.5 Hz and 6 Hz.

Figure 5 shows the recorded output voltage from the piezoelectric element for the resonant frequency $f$ = 2.75 Hz at the given air flow velocity $v$ = 6 m/s. This measurement point corresponds to the highest voltage generated by the tested piezoelectric element. The measurement time for each of the cases was 30 s.

Figure 6 shows a sample measured acceleration signal of the test object as a function of time. Each of the recorded measurement points is composed of samples recorded over 30 s with a sampling rate of 800 Hz. In order to clarify, the vibration signals, which are put into the analysis are collected from the tip of the bluff-body. The acceleration of the beam is directly coupled with the generated voltage from the beam's deflection. The response of both acceleration and output voltage time-series are similar to each other, what is shown in the further part of the research (Figure 8 and Figure 9.)

Figure 7 compares the G force for the given excitation and the system response indicated as

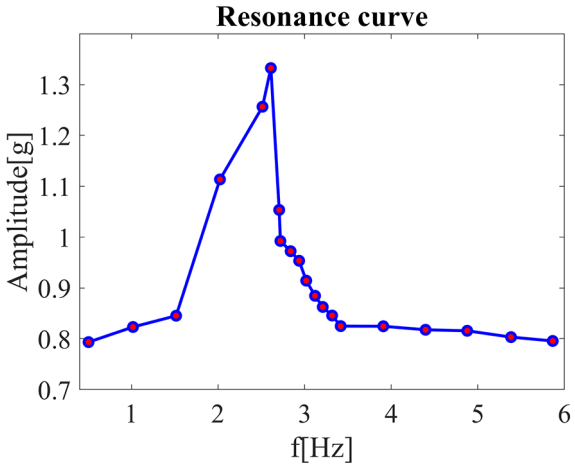


**Fig. 4.** The maximum G force for the moving bluff-body as a function of natural frequency $f$ – the case with no air flow in the wind tunnel

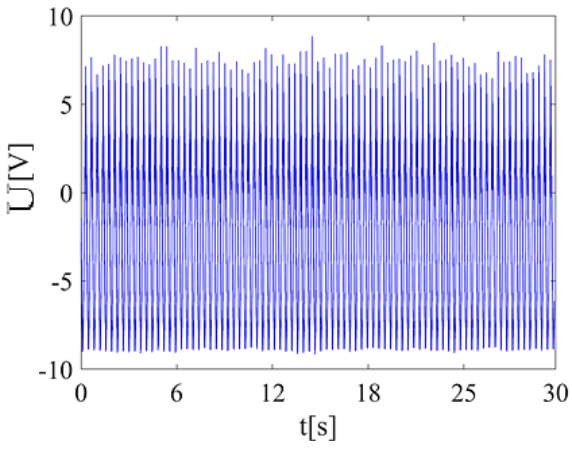


**Fig. 5.** The output voltage for the resonance frequency $f$ = 2.75 Hz at the given air flow velocity v=6 m/s

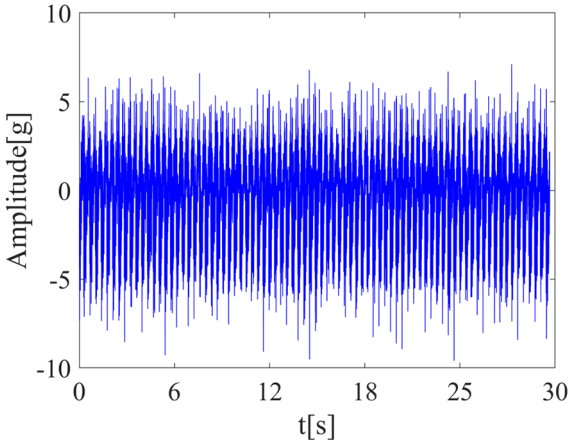


**Fig. 6.** The amplitude of the G force as a function of time for the resonance frequency $f$ = 2.75 Hz at the given air flow velocity v=6 m/s

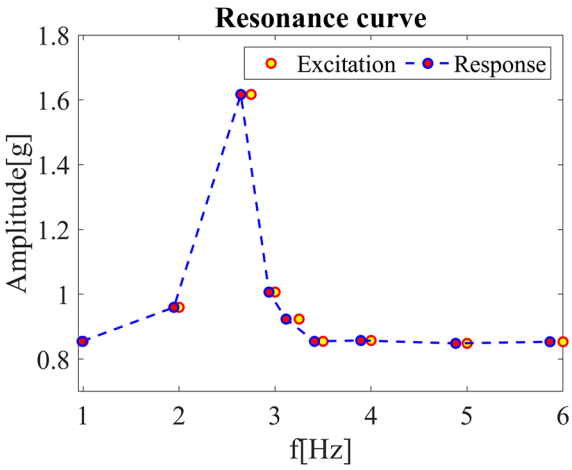


**Fig. 7.** The G force for the given excitation and system's responses

the Response. The given frequency was achieved with a TIRA DA 200 digital amplifier. The Response value was a signal measured with an accelerometer installed where the sting was mounted on the holder of a TIRA S513 vibration generator. A characteristic shift in the system's response for the given forcing was observed. The system obtained minimally higher vibration frequencies below the resonant frequency but above the resonant frequency, it vibrated with a lower frequency. The observed phenomenon is related to the fact that the whole bluff-body on the beam is mounted on the support needed to put it into the testing chamber in airflow tunnel. The shift of frequency of the excitation and the system's frequency is quite small despite the fact of mounting the system on the support. However, to completely eliminate mention shift in the future tests, we plan to make the support more rigid to have the same frequency of the excitation and at the bluff-body. The maximum G force equal to 1.6 was recorded for a forcing frequency of $f$ = 2.75 Hz. For the extreme values of $f_{min}$ = 1 Hz and $f_{max}$ = 6 Hz, the G force was 0.85. A positive impact of an increase in the G force by about 20% at the resonant frequency and by about 7.6% at $f_{min}$ and $f_{max}$ was recorded as compared to the discussed case with no air flow in the wind tunnel.

Figure 8 shows the voltage on the piezoelectric element as a function of air flow velocity for the test bluff body. For all excitation frequencies except $f_3$ = 2.75 Hz, the generated voltage specified by an increasing function over the entire range increased. For $f_3$, on the other hand, the function that specifies the generated voltage at first increases (up to 6.0 m/s) and then decreases even to 10 m/s if the velocity of 9 m/s at which a sudden drop in voltage occurred were ignored. Despite

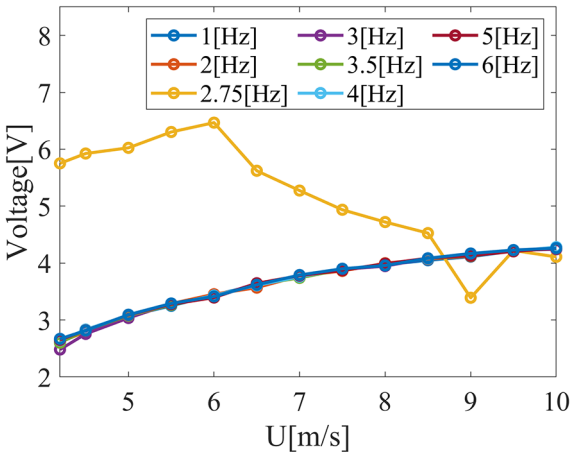


**Fig. 8.** The RMS voltage on the piezoelectric element as a function of air flow velocity for the given bluff body

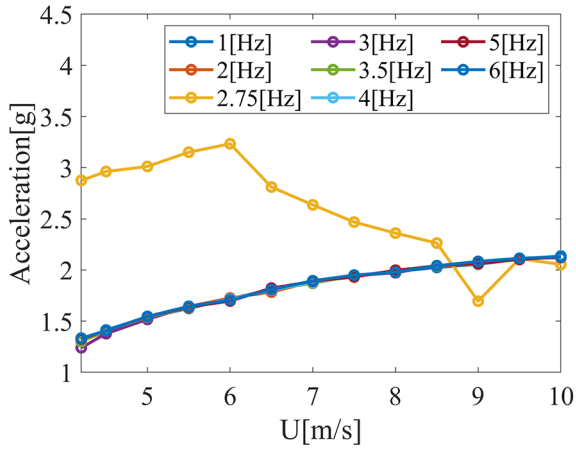


**Fig. 9.** Acceleration of the end of the cantilever beam with the piezoelectric element as a function of air velocity for the considered bluff body

voltage was generated over the entire range of the given velocity at all excitation frequencies, it was definitely the range of 4.2–8.5 m/s the highest voltage was recorded at $f_3$ = 2.75 Hz. For this frequency, a maximum voltage of 6.47 V was recorded at a wind velocity of 6 m/s. This voltage is 89% higher than the average voltage generated by the piezoelectric material at the other frequencies. This is relatively good compared to the results in the paper [14] where among the results obtained, only for $m_1$ and $f$ = 4 Hz did the bluff body vibrate with a large amplitude over the entire range of airflow velocities. For the other considered configurations, the bluff body did not vibrate so intensively at velocities below 8 or 9 m/s.

From the perspective of the Energy Harvesting, there is the focus on getting the highest possible output voltage/power level. In our case it is obtained by the specific value the wind velocity and the excitation at the mechanical vibrations shaker. What is worth mentioning that the oscillation solution is obtained by the frequency $f_3$ = 2.75 Hz, however this frequency of internal resonance of the system can be easily changed by the position of additional springs that are coupled with the oscillating beam.

The RMS acceleration of the moving bluff-body as a function of air flow velocity, just like the generated voltage, showed an identical tendency (Fig. 9).

## CONCLUSIONS

The bluff body vibrates over the entire range of the given air flow velocity. Except for the case with the excitation frequency of $f_3$ = 2.75 Hz, almost identical characteristics of voltage and acceleration as a function of air flow velocity in the wind tunnel were obtained. The highest voltage generated by the piezoelectric element was recorded for this frequency for the velocity range from $v$ = 4.2 m/s to $v$ = 8.5 m/s because $f_3$ = 2.75 Hz was the resonant frequency of the tested system. The piezoelectric element can be maximally used if the operating point corresponding to the resonant frequency is selected. Compared to the previous experiments, the optimal mechanical solution has been found by adding side springs so that an oscillatory solution at both high and low wind speeds has been achieved. If this trend is continued, the impact of the configuration of additional springs on optimizing the system's performance in the wind tunnel will be investigated in future research. The optimization problem will be directed to scavenging the highest possible output voltage/power and how its divers with the change of internal frequency of the system. The change of internal frequency will be the result of different mass and the alignment of the additional springs.

Observing the potential of the system, it can be applied in the external environment. For instance, it can be applied as the coupling with rotating blade [25], in structural health monitoring (SHM) in buildings [26] or used by the side of highways, where the wake-induced vibration phenomena is observed by cars [27]. One of potential ways it can be the coupling of the system with unmanned aerial vehicles (UAVs) for powering the low-demanding sensors [28, 29].

### Acknowledgements

Publication was supported by the program of the Polish Ministry of Science and Higher Education under the project DIALOG 0019/DLG/2019/10 in the years 2019–2021.

## REFERENCES

1. Safaei M., Sodano H.A., Anton S.R. A review of energy harvesting using piezoelectric materials: State-of-the-art a decade later (2008–2018). Smart Materials and Structures. 2019; 28(11): 113001.
2. Salazar M., Serrano M., Abdelkefi A. Fatigue in piezoelectric ceramic vibrational energy harvesting: A review. Applied Energy. 2020; 270: 115161.
3. Wang J., Gu S., Zhang C., Hu G., Chen G., Yang K., Li H., Lai Y., Litak G., Yurchenko D. Hybrid wind energy scavenging by coupling vortex-induced vibrations and galloping. Energy Conversion and Management. 2020; 213: 112835.
4. Ambrożkiewicz B., Litak G., Wolszczak P. Modelling of electromagnetic energy harvester with rotational pendulum using mechanical vibrations to scavenge electrical energy. Applied Sciences. 2020; 10(2): 671.
5. Zhang H., Sui W., Yang C., Zhang L., Song R., Wang J. An asymmetric magnetic-coupled bending-torsion piezoelectric energy harvester: Modeling and experimental investigation. Smart Materials and Structures. 2022; 31(1): 015037.
6. Guo X., Zhang Y., Fan K., Lee C., Wang F. A comprehensive study of non-linear air damping and "pull-in" effects on the electrostatic energy harvesters. Energy Conversion and Management.

2020; 203: 112264.

7. Nozariasbmarz A., Collins H., Dsouza K., Polash M.H., Hosseini M., Hyland M., Liu J., Malhotra A., Ortiz F.M., Mohaddes F., Ramesh V.P., Sargolzaeiaval Y. Review of wearable thermoelectric energy harvesting: From body temperature to electronic systems. Applied Energy. 2020; 258: 114069.
8. Sezer N., Koc M. A comprehensive review on state-of-the-art of piezoelectric energy harvesting. Nano Energy. 2021; 80: 105567.
9. Dong K., Peng X., Wang Z.L. Fiber/Fabric-Based Piezoelectric and Triboelectric Nanogenerators for Flexible/Stretchable and Wearable Electronics and Artificial Intelligence. Advanced Materials. 2020; 32(5): 1902549.
10. Iqbal M., Nauman M.M., Khan F.U., Abas P.E., Cheok Q., Iqbal A., Aissa B. Vibration-based piezoelectric, electromagnetic, and hybrid energy harvesters for microsystems applications: A contributed review. International Journal of Energy Research. 2021; 45(1): 65–102.
11. Zou H-X., Li M., Zhao L-C., Gao Q-H., Wei K-X., Zuo L., Qian F., Zhang W-M. A magnetically coupled bistable piezoelectric harvester for underwater energy harvesting. Energy. 2021; 217: 119429.
12. Aravindan M., Ali S.F. Exploring 1:3 internal resonance for broadband piezoelectric energy harvesting. Mechanical Systems and Signal Processing. 2021; 153: 107493.
13. Huguet T., Badel A., Druet O., Lallart M. Drastic bandwidth enhancement of bistable energy harvesters: Study of subharmonic behaviors and their stability robustness. 2018; 226: 607–617.
14. Ambrożkiewicz B., Czyż Z., Karpiński P., Stączek P., Litak G., Grabowski Ł. Ceramic-Based Piezoelectric Material for Energy Harvesting Using Hybrid Excitation. Materials. 2021; 14: 5816.
15. Shengxi Z., Wang J. Dual serial vortex-induced energy harvesting system for enhanced energy harvesting. AIP Advances. 2018; 8(7): 075221.
16. Yang K., Wang J., Yurchenko D. A double-beam piezo-magneto-elastic wind energy harvester for improving the galloping-based energy harvester. Applied Physics Letters. 2019; 115(19): 5126476.
17. Zhang M., Yang S., Abdelkefi A., Yu H., Wang J. Vortex-induced vibration of a circular cylinder with nonlinear stiffness: prediction using forced vibration data. Nonlinear Dynamics. 2022; 108(3): 1867–1884.
18. Javed U., Abdelkefi A. Role of the galloping force and moment of inertia of inclined square cylinders on the performance of hybrid galloping energy harvesters. Applied Energy. 2018; 231: 259–276.
19. Toyabur R.M., Salauddin M., Cho H., Park J.Y. A multimodal hybrid energy harvester based on piezoelectric-electromagnetic mechanisms for low-frequency ambient vibrations. Energy Conversion and Management. 2018; 168: 454–466.
20. Cao Y., Huang H. Performance optimization and broadband design of piezoelectric energy harvesters based on isogeometric topology optimization framework. European Journal of Mechanics. A/Solids. 2023; 97: 104800.
21. Li X., Yurchenko D., Li R., Feng X., Yan B., Yang K. Performance and dynamics of a novel bistable vibration energy harvester with appended nonlinear elastic boundary. Mechanical Systems and Signal Processing. 2023; 185: 109787.
22. Sharghi H., Bilgen O. Dynamics of pendulum-based systems under human are rotational movements. Mechanical Systems and Signal Processing. 2023; 183: 109630.
23. Kan J., Wang J., Meng F., He C., Li S., Wang S., Zhang Z. A downwind-vibrating piezoelectric energy harvester under the disturbance of a downstream baffle. Energy. 2023; 262: 125429.
24. https://www.smart-material.com/media/Presentations/K-Wilkie-ISMA-2005.pdf (26.08.2021).
25. Zou H., Cai F., Zhang J., Chu Z. Overview of environmental airflow energy harvesting technology based on piezoelectric effect. Journal of Vibroengineering. 2022; 24(1): 91–103.
26. Matiko J.W., Grabham N.J., Beeby S.P., Tudor M.J. Review of the application of energy harvesting in buildings. Measurement Science and Technology. 2014; 25(1): 012002.
27. Yan Z., Shi G., Zhou J., Wang L., Zuo L., Tan T. Wind piezoelectric energy harvesting enhanced by elastic-interferred wake-induced vibration. Energy Conversion and Management. 2021; 249: 114820.
28. Czyż Z., Karpiński P., Stryczniewicz W. Measurement of the flow field generated by multicopter propellers. Sensors. 2020; 20(19): 5537.
29. Koszewnik A. Assessment parameters of fractional order capacitor of piezo-patch harvester located on a multicopter. European Physical Journal: Special Topics. 2022; 231(8): 1505–1516.